Neuron, Volume *109*

Supplemental information

Hippocampal ripples and their coordinated dialogue with the default mode network during recent and remote recollection

Yitzhak Norman, Omri Raccah, Su Liu, Josef Parvizi, and Rafael Malach


right hipp.
left hipp.
P
A
CA1
CA2/3
Subiculum
Distance (mm)
Patient 1
LB1 LC3 LC2 LC1
Patient 2
LAH1 RAH3 RAH2 RAH1 RPH3 RPH2 RPH1
Patient 3
RmHIP3 RmHIP2 RmHIP1 LaHIP4 LaHIP3 LaHIP2 LaHIP1 LAmy1
Patient 4
LHA4 LHA3 LHA2 LHA1 LMH3 LMH2 LMH1 LPH4 LPH3 LPH2
Patient 5
RAMY4 RAMY3 RAMY2 RAMY1 LAMY3 LAMY2 LAMY1 RPMT3 RPMT2
Patient 6
RAH3 LAH2 LAH1
Patient 7
RAH4 RAH3 RAH2
Patient 8
LAT2 LAT1
Patient 9
LH3 LH2 RH2 RH1
Patient 10
RAH3 RAH2 RMH1
Patient 11
RH2 RAM1 LH3 LH2 LH1
Patient 12
RMH3 RMH2 RMH1 LMH4 LMH2 LMH1
Patient 13
LA2 LH2 LH1
Patient 14
LHIP3 LHIP2 LHIP1 RAH3 RAH2 RAH1
Patient 15
RSTA2 RSTA1 RPH2 RPH1
Patient 16
N/A
RHP4 RHP3 RHP2 RHP1 LAMY4 LAMY3 LAMY2 LHP4 LHP3 LHP2
Patient 17
LPH2 RPH2 RPH1 RMH5 RMH4 RMH3 RMH2 RMH1 LMH4 LMH3 LMH2 LMH1
Patient 18
LH2 RH4 RH3 RH2 RH1
Patient 19
RAH2 RAH1
Patient 20
RAH4 RAH3 RAH2 RAH1 LHH4 LHH3 LHH1

Figure S1. Anatomical location of hippocampal recording sites in each patient, related to Figure 1

The two hippocampi were reconstructed in the native space of each patient's brain using the hippocampal subfields parcellation algorithm included in Freesurfer (Iglesias et al., 2015). Individual electrode contacts were identified and marked on the co-registered CT scan (see Methods), and plotted on the reconstructed hippocampi (red spheres). The accompanying bar charts show the distance of each contact from CA1, CA2/3 and subiculum subfields (the main stations on the hippocampus output pathway). Only electrodes located within 2 mm from one of these subfields were included in the analysis and were subjected to ripple detection. (A - anterior; P - posterior)

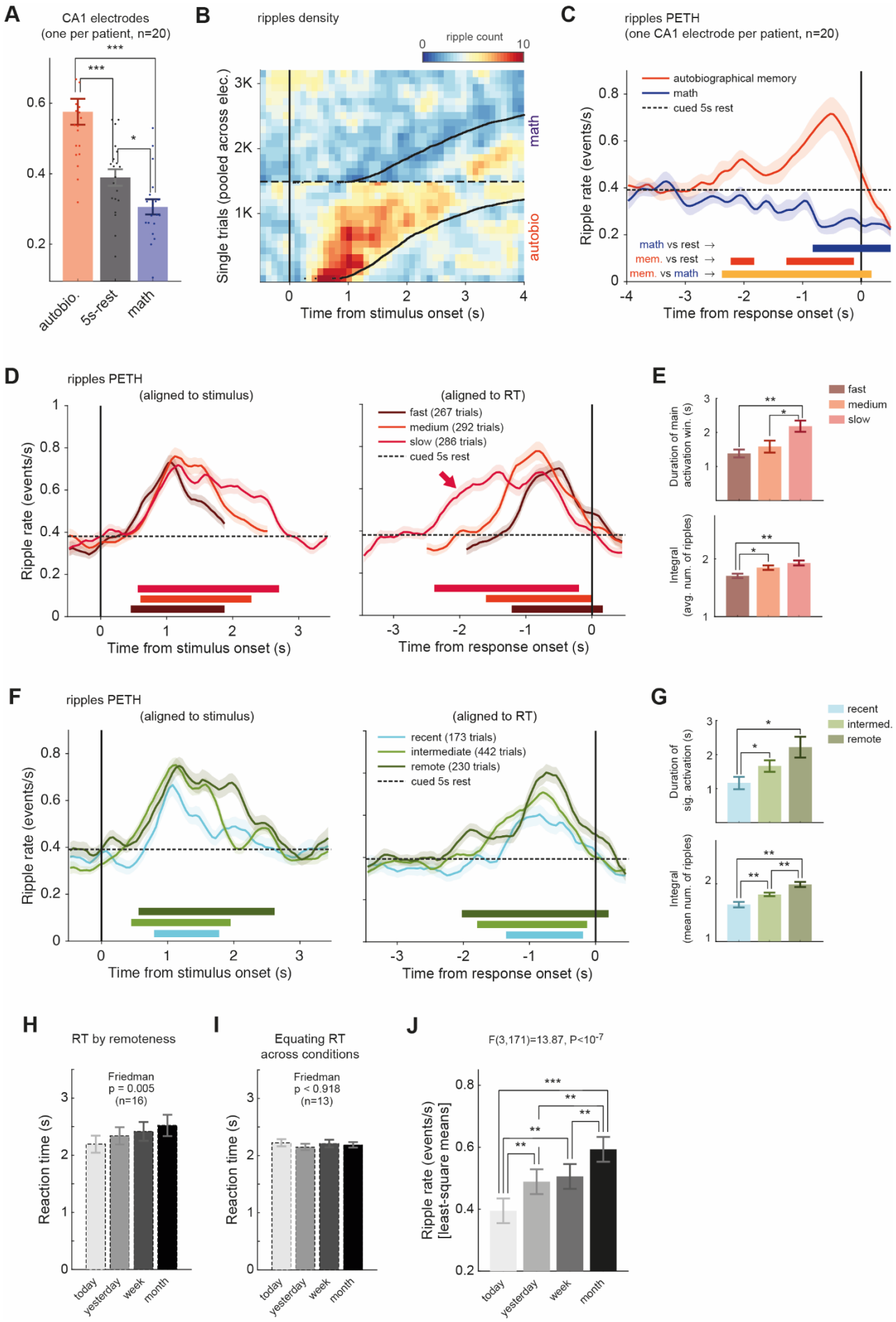
A
CA1 electrodes
(one per patient, n=20)
***
***
*
0.6
0.4
0.2
autobio.
5s-rest
math
B
ripples density
ripple count
0
10
3K
2K
1K
Single trials (pooled across elec.)
math
autobio
0
1
2
3
4
Time from stimulus onset (s)
C
ripples PETH
(one CA1 electrode per patient, n=20)
autobiographical memory
math
cued 5s rest
Ripple rate (events/s)
0.8
0.6
0.4
0.2
0
math vs rest →
mem. vs rest →
mem. vs math →
-4
-3
-2
-1
0
Time from response onset (s)
D
ripples PETH
(aligned to stimulus)
(aligned to RT)
fast (267 trials)
medium (292 trials)
slow (286 trials)
cued 5s rest
Ripple rate (events/s)
1
0.8
0.6
0.4
0.2
0
0
1
2
3
Time from stimulus onset (s)
-3
-2
-1
0
Time from response onset (s)
E
fast
medium
slow
Duration of main activation win. (s)
3
2
1
**
*
Integral (avg. num. of ripples)
2
1
*
**
F
ripples PETH
(aligned to stimulus)
(aligned to RT)
recent (173 trials)
intermediate (442 trials)
remote (230 trials)
cued 5s rest
Ripple rate (events/s)
0.8
0.6
0.4
0.2
0
0
1
2
3
Time from stimulus onset (s)
-3
-2
-1
0
Time from response onset (s)
G
recent
intermed.
remote
Duration of sig. activation (s)
3
2
1
*
*
Integral (mean num. of ripples)
2
1
**
**
**
H
RT by remoteness
Friedman
p = 0.005
(n=16)
Reaction time (s)
3
2
1
0
today
yesterday
week
month
I
Equating RT
across conditions
Friedman
p < 0.918
(n=13)
Reaction time (s)
3
2
1
0
today
yesterday
week
month
J
F(3,171)=13.87, P<10-7
Ripple rate (events/s)
[least-square means]
0.8
0.6
0.4
0.2
***
**
**
**
**
today
yesterday
week
month

Figure S2. Group-level results using a single hippocampal electrode in each patient, related to Figure 2

(A) Group-level results showing mean ripple rate across the main experimental conditions when using only one hippocampal site in each patient (the electrode closest to CA1 subfield). Dots represent individual patients/electrodes. Error bars represent SEM across patients (n=20). Accompanies Figure 2 (main-text).

(B) Ripples density plot showing increase/decrease in ripple probability following autobiographical/math statements, respectively. Trials were pooled together across all electrodes and sorted according to reaction time (black curve). Ripples density was computed in bins of 100 ms × 100 trials, smoothed using a 3-bins-wide Gaussian filter for visualization purposes. Note that the transient increases in ripple probability closely tracked reaction times.

(C) Peri-event Time Histogram (PETH) of ripples aligned to the patient's response. Note the significant decrease in ripple rate during math (blue) and a significant increase during autobiographical retrieval (red), peaking 600 ms prior to the patient's response.

(D) Ripples activation profiles across reaction time (RT) categories. Autobio trials were pooled across recording sites and grouped according to the RTs. We used the 2nd, 3rd and 4th RT quintiles to select fast, medium and slow trials, discarding more extreme RTs (i.e., 1st and 5th quintiles). PETHs of ripples were computed individually for each RT category, relative to stimulus onset (left) and to the patient's response (right). Horizontal lines above the x-axis indicate the largest temporal cluster in which ripple rate was significantly greater than rest ($P<0.05$, bootstrap test). Shaded areas represent bootstrap SE over trials (pooled across all electrodes). Note clear indication for pre-recall ripple activation in the slow RT category (arrow).

(E) Slow trials exhibited longer activations and overall higher number of ripples elicited per trial (i.e., area under the response curve) compared to faster trials (*$P<0.05$, ** $P<0.01$; bootstrap test). Error bars represent bootstrap SE over trials, pooled across all electrodes.

(F) Ripple activation profile varies with memory remoteness. Autobio trials were pooled across recording sites and grouped by remoteness level: memories from today (recent), yesterday/last week (intermediate) and last month (remote). PETHs of ripples were computed individually in each trial group, either relative to stimulus onset (left) or to the patient's response (right). As in D, trials belonging to the first and last RT quintiles were excluded from analysis (for consistency). Horizontal lines above the x-axis and shaded areas represent the same as in D.

(G) Ripple activation during remote recollections lasted longer and generated more ripples overall (i.e., area under the response curve) compared to more recent recollections (*$P<0.05$, ** $P<0.01$; bootstrap test). Error bars represent the same as in E.

(H) Reaction times increased significantly with remoteness level ($P=0.005$, Friedman test, n=16 patients). A post-hoc comparison indicated significantly longer RTs for remote compared to recent memories (last month vs today: $P=0.003$, Wilcoxon signed-rank test).

(I) To control for RT differences as a possible confounding factor mediating the relationship between remoteness and ripple rate (Figure 2G), we equated reaction times across conditions through the following steps: transforming RT values to z-scores (relative to the mean and variance of RT in each patient); discarding outlier trials (RT > 3SD); and selecting trials in such manner that equalizes RT across conditions.

(J) Comparing ripple rate across remoteness levels under equal RTs, revealed a significant increase in ripple rate with remoteness (mixed effects analysis similar to the one reported in Figure 2G: $F(3,171)=13.87$, $P<10^{-7}$; n=13 patients; post-hoc comparisons: * $P<0.05$, ** $P<0.01$, *** $P<0.001$, FDR corrected). Notably, these results demonstrate that memory remoteness significantly affects ripple rate, regardless of RT. Error bars represent SEM estimated by the mixed-effects model.

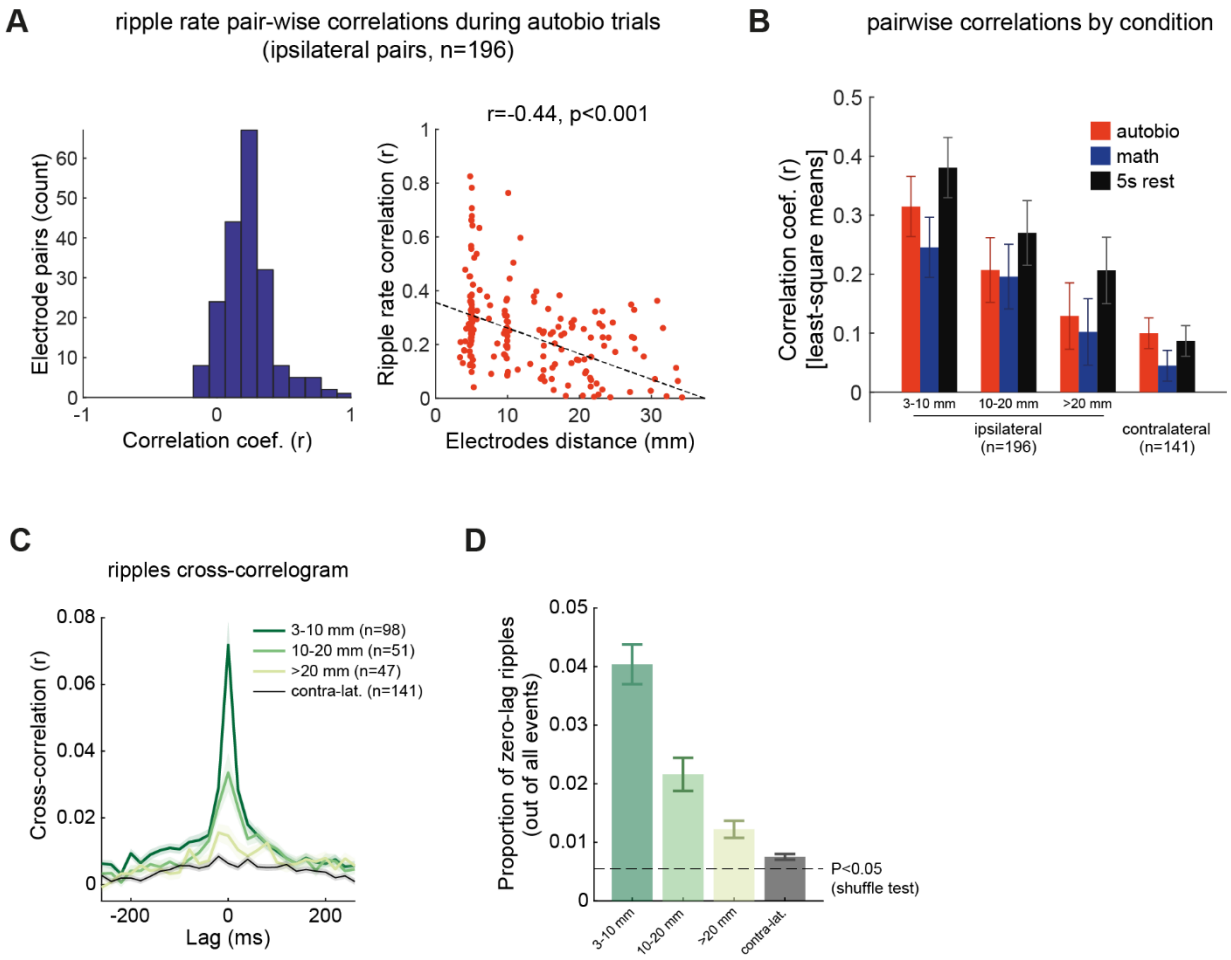

Figure S3. Trial-to-trial ripple rate correlations and ripple coincidence analysis across neighboring hippocampal electrodes demonstrating the local nature of ripple activation, related to Figure 2.

(A) Trial-to-trail correlation between ripple rates measured in neighboring electrodes during autobio trials. Left panel shows the distribution of correlation coefficients across all ipsilateral electrode pairs (n=196). Right panel shows that the magnitude of the correlation decreased significantly as a function of the inter-contact distance (right panel; r=-0.44, P<0.001).

(B) Following Fisher transformation, correlation coefficients across ipsilateral pairs were entered into a mixed effects model formulated as follows: Correlation ~ Distance × Condition + (1|Patient / Electrode pair). 'Distance' and 'Condition' are categorical variables with three levels each (Distance: '0-10mm', '10-20mm', '>20mm'; Condition: 'autobio', 'math', '5s rest'). 'Patient' and 'Electrode-pair' were treated as a nested random factor, accounting for the fact that different participant contributed a different number of electrodes to the analysis. Contralateral pairs were analyzed in a similar model, but without a fixed factor of Distance. The results revealed significant effects of distance (ipsilateral: $F(2,177.21)=30.86$, $P<10^{-11}$), and condition (ipsilateral: $F(2,19.01)=P<10^{-7}$; contralateral: $F(2,280)=0.004$, $P<0.004$), with no significant interaction. Post hoc comparisons indicated that the correlation between ipsilateral pairs was significantly higher during rest compared to the other conditions (rest-vs-autobio: $t(386)=4.01$,$P=0.0001$; rest-vs-math: $t(386)=6.06$,$P<10^{-8}$). In contralateral pairs the correlation was significantly lower during math compared to the other two conditions (math-vs-rest: $t(280)=-2.46$, $P<0.02$; math-vs-autobio: $t(280)=-3.23$, $P<0.005$). All pairwise t-tests were FDR corrected. Error bars represent SEM estimated by the mixed-effects model.

(C) Coincidence of ripples across electrode pairs. We used the timestamps of the ripples' peak during autobio trials, to produce cross-correlograms between different electrode pairs within the hippocampus (among the electrodes that were subjected to ripple detection, see Methods). The results indicated an increase in cross-correlation peaking around zero-lag. This cross-correlation rapidly diminished as a function of the inter-contact distance.

(D) To quantify the actual prevalence of coincident ripple activation (i.e., ripples that emerged simultaneously on two electrodes), we calculated the proportion of overlapping (zero-lag) ripples out of the total number of ripples detected in

each pair of electrodes. The results indicated a significant but minor prevalence of ripple coincidences of up to 4% in the most adjacent electrodes ($P<0.01$, compared to chance-level computed by shuffling ripple timestamps between trials). It should be noted that excluding from the analysis recording sites that shared the same white matter reference did not significantly change the results (data not shown).

For the analysis in C and D we used 20 ms bins. Error bars represent SEM.

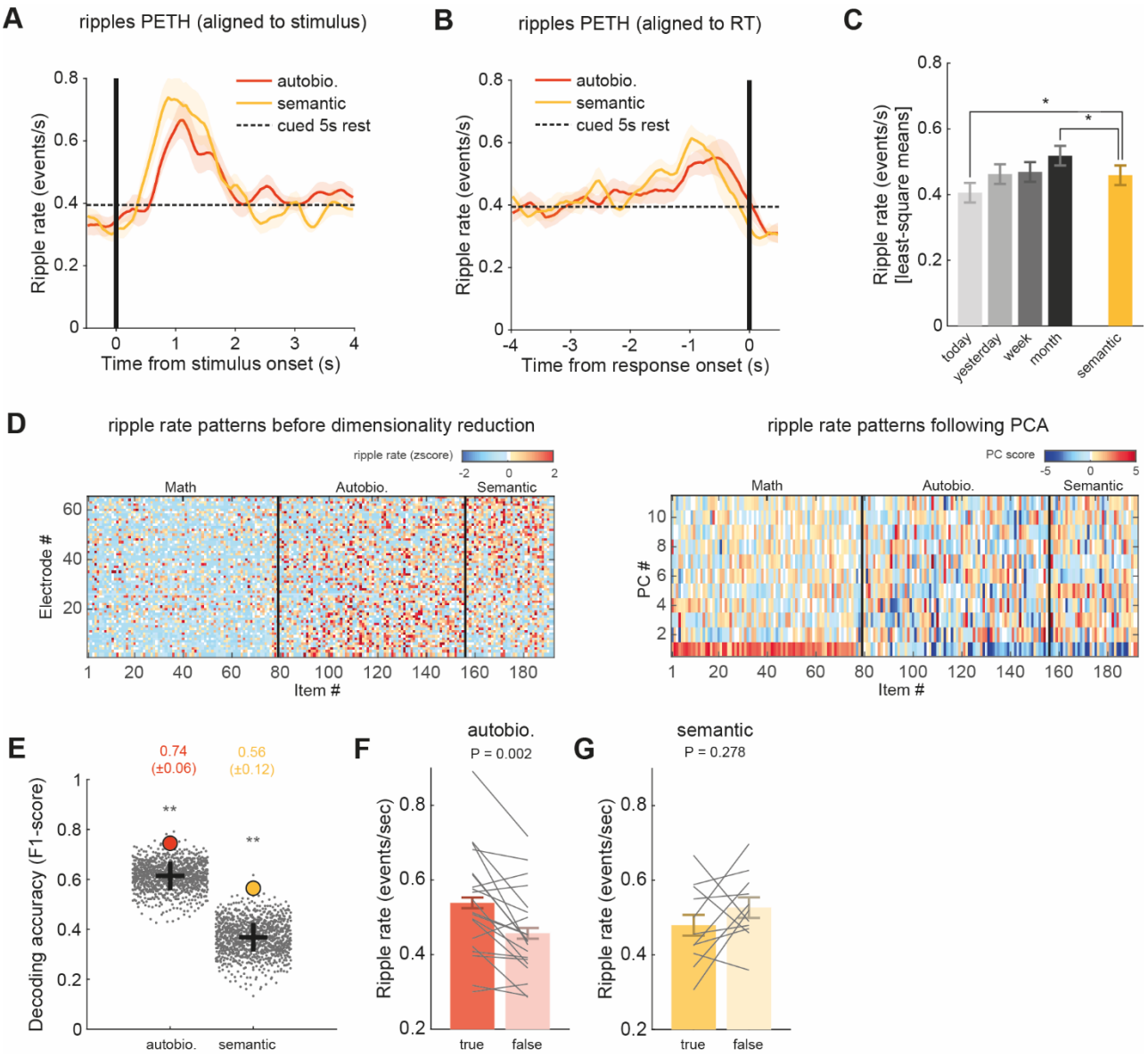

Figure S4. Supplemental multivariate and univariate ripple-rate analyses across autobiographic and semantic trials, related to Figures 3 & 4

(A-B) Comparing the dynamics of hippocampal ripples emergence during the autobio and semantic conditions did not reveal a significant difference between the two conditions, neither when aligning the ripple peri-event time histogram to stimulus onset nor when aligning it to reaction time. Shaded areas represent SEM across patients.

(C) Mixed effects analysis similar to the one reported in Figure 2G, applied to data from the 11 patients that had both the autobio and semantic conditions. Post-hoc pair-wise comparisons indicated that semantic memory was significantly lower compared to the most remote autobiographical memories (experiences from the last month) and significantly higher compared to the most recent autobiographical memories (experiences from today). Thus, the overall ripple rate by itself could not account for the gradual transition from autobio-to-semantic revealed by the pattern similarity analysis in Figure 4.

(D) Depiction of multivariate ripple rate patterns across 65 electrodes in 11 patients with autobio and semantic conditions, before and after dimensionality reduction using Principal Component Analysis (PCA). Each column in these two matrices corresponds to one statement, e.g. "I ate an apple yesterday" (autobio), "Babe Ruth was a football player" (semantic) or "44 + 9 = 51" (math). The rows correspond to individual electrodes in the left panel, and to principal components in the right panel.

(E) A linear discriminant analysis classifier, similar to the one reported in Figure 3, was trained to discriminate only between autobio and semantic trials (excluding math). Here too, classification performance (F1-scores) was highly significant (autobio: 0.74 ± 0.06; semantic: 0.56 ± 0.12; SEM was computed using a Jack knife procedure, excluding one patient at a time). Filled circles denote the actual result, gray dots show results for same data when trial labels were randomly shuffled. Gray crosses indicate chance level in each class.

(F) Bar-plots of ripple rates for autobiographical statements reported as TRUE vs. those reported as FALSE. Ripple rate was computed in a 2 s time window centered on the peak of the grand-average autobio response. The results show preferential ripple activation for TRUE responses (P=0.002, Wilcoxon signed rank test; n=20 patients).

(G) Ripple rate across TRUE and FALSE semantic statements. Ripple rate was computed in a 2 s time window centered on the peak of the grand-average semantic response. No significant difference was found (P=0.278, Wilcoxon signed rank test; n=11 patients). Error bars in F and G represent the 95% confidence interval of the within-subject difference(Loftus and Masson, 1994).

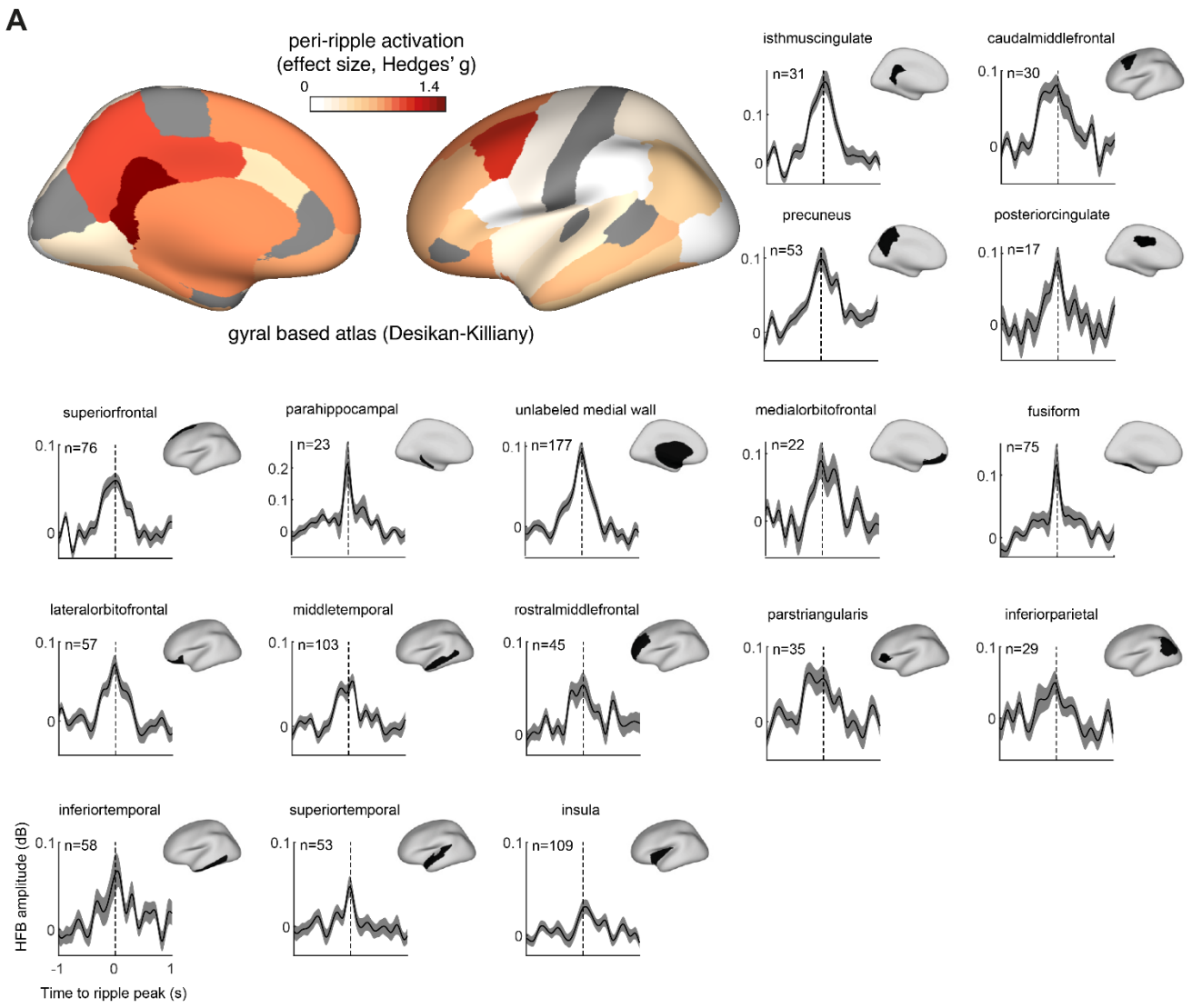
A
peri-ripple activation
(effect size, Hedges' g)
0
1.4
gyral based atlas (Desikan-Killiany)
isthmuscingulate
n=31
caudalmiddlefrontal
n=30
precuneus
n=53
posteriorcingulate
n=17
superiorfrontal
n=76
parahippocampal
n=23
unlabeled medial wall
n=177
medialorbitofrontal
n=22
fusiform
n=75
lateralorbitofrontal
n=57
middletemporal
n=103
rostralmiddlefrontal
n=45
parstriangularis
n=35
inferiorparietal
n=29
inferiortemporal
n=58
superiortemporal
n=53
insula
n=109
HFB amplitude (dB)
Time to ripple peak (s)

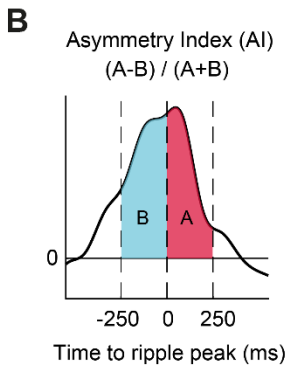
B
Asymmetry Index (AI)
(A-B) / (A+B)
B
A
-250
0
250
Time to ripple peak (ms)

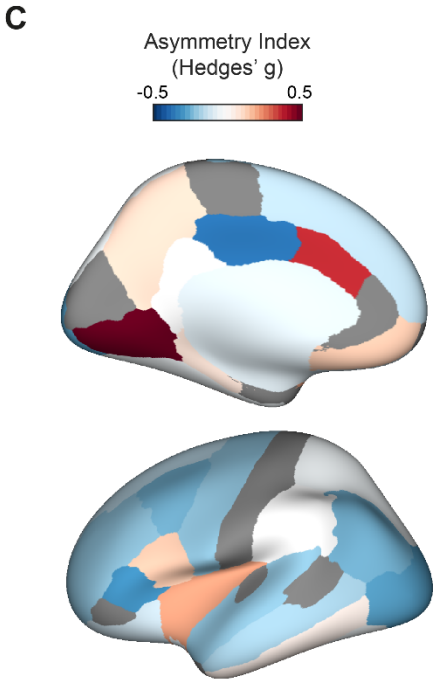
C
Asymmetry Index
(Hedges' g)
-0.5
0.5

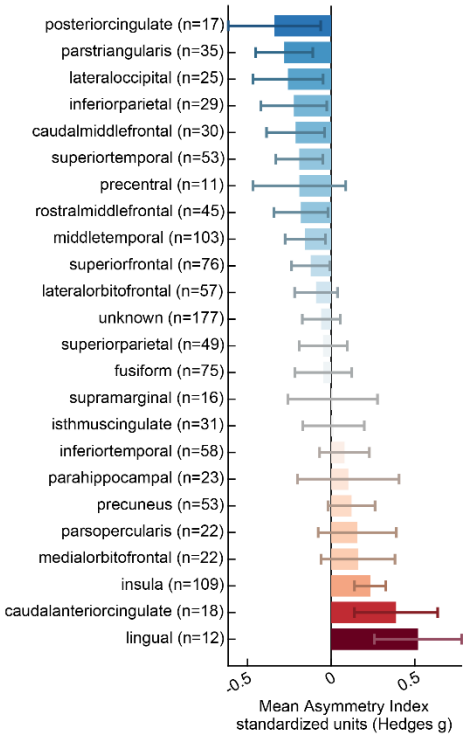
posteriorcingulate (n=17)
parstriangularis (n=35)
lateraloccipital (n=25)
inferiorparietal (n=29)
caudalmiddlefrontal (n=30)
superiortemporal (n=53)
precentral (n=11)
rostralmiddlefrontal (n=45)
middletemporal (n=103)
superiorfrontal (n=76)
lateralorbitofrontal (n=57)
unknown (n=177)
superiorparietal (n=49)
fusiform (n=75)
supramarginal (n=16)
isthmuscingulate (n=31)
inferiortemporal (n=58)
parahippocampal (n=23)
precuneus (n=53)
parsopercularis (n=22)
medialorbitofrontal (n=22)
insula (n=109)
caudalanteriorcingulate (n=18)
lingual (n=12)
Mean Asymmetry Index
standardized units (Hedges g)

Figure S5. Peri-ripple activity during autobiographical recall in gyral-based ROIs, related to Figure 5

(A) Deconvolved peri-ripple HFB activity averaged over gyral-based regions of interest (ROIs) defined using the Desikan-Killiany atlas (Desikan et al., 2006). The panel in the top-left corner depicts the magnitude of peri-ripple activation (Hedges' g effect size) in a time window of -250 to 250 ms relative to the hippocampal ripple peak. Areas sampled by less than 10 electrodes were excluded from the analysis and were painted in gray. Note, when assigning bipoles to a certain region, we only required that at least one of the two contacts be located within that region, thus allowing for the same bipole to be attributed to two different regions (in cases where the bipole was located on the border between regions). Shaded areas represent SEM.

(B) To examine potential asymmetries in the peri-ripple cortical activity relative to ripple peak, we followed the method described in (Karimi Abadchi et al., 2020) and calculated an Asymmetry Index (AI): the difference between mean HFB activity in intervals of 250 ms after and before ripple peak, divided by their sum. Positive and negative AI values reflect cortical activation that tends to follow or to precede the ripple event, respectively.

(C) Summary of AI values across the gyral-based ROIs described in panel A. The values are presented in standardized units (Hedges' g effect size, relative to zero). Areas that showed stronger activity before the ripple appear in blue shades; areas that showed stronger activity following the ripple appear in red shades; and areas where peri-ripple activity was symmetrical with respect to ripple peak appear in white. Areas sampled by less than 10 electrodes were excluded from the analysis and were painted in gray. Error bars represent SEM.

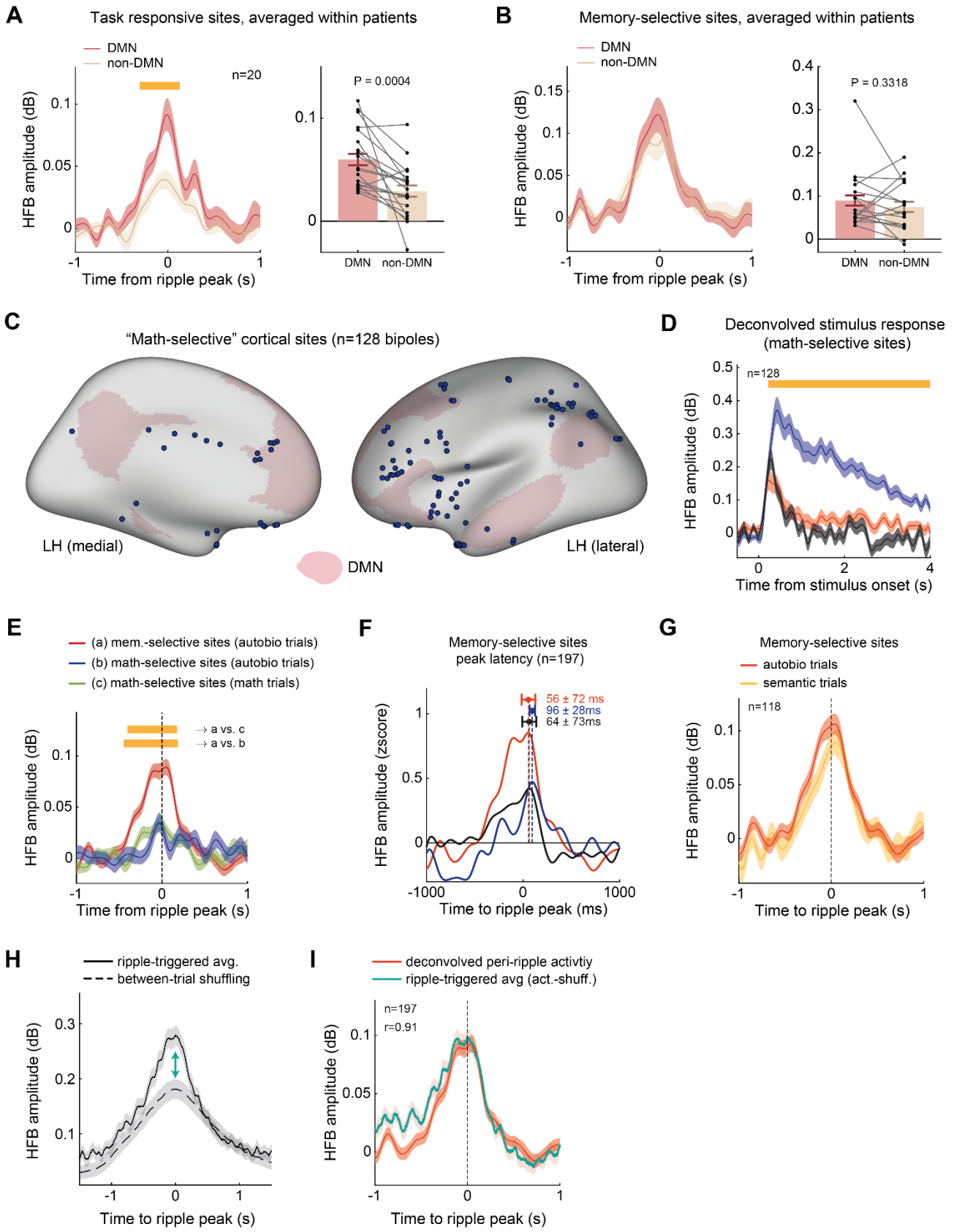

Figure S6. Peri-ripple cortical responses in memory-selective sites (DMN versus non-DMN) and in math-selective sites, related to Figures 5 & 6

(A) Within-subjects analysis of deconvolved peri-ripple HFB responses across task-responsive sites, within versus outside the DMN. This analysis generalizes the effect depicted in Figure 5D across the different participants. Left: HFB

activation profile in each electrode group. A non-parametric cluster-based permutation test indicated higher HFB activity in DMN sites ($P<0.01$, n=20 patients; orange horizontal bar indicates significant time points). Right: single subject data of HFB amplitude in a time window of -250 to 250 relative to ripple peak ($P<0.001$, Wilcoxon signed rank test, n=20 patients).

(B) Same as in A, but in "memory-selective" sites. Note, peri-ripple activation profiles were comparable across memory-selective sites, both inside and outside the DMN. This suggests that peri-ripple activity during recall is not limited to the DMN per-se, but rather extends to additional cortical sites involved in memory processes (left panel: P=NS, n=17 patients; right panel: P=0.33, n=17 patients).

(C-E) A control analysis supplementing Figure 6 (main text), showing peri-ripple responses in an ensemble of 'math-selective' cortical sites. Panel C depicts the anatomical locations of math-selective sites (i.e. electrodes showing a significant preference to math compared to autobio; $P<0.05$ FDR adjusted, n=128 bipoles). Panel D shows the deconvolved stimulus-response in those sites (math in blue, autobio in red and 5-sec rest in black). Panel E shows the deconvolved peri-ripple response during autobio and math trials. Compared to the peri-ripple activity exhibited in the memory-selective sites during the autobio condition (also reported in Figure 6C), peri-ripple responses in math-selective sites were significantly weaker ($P<0.001$, cluster-based permutation test). Orange horizontal bar indicates significant time points.

(F) Using a bootstrap sampling procedure with 2,000 resamples we estimated the latency of peri-ripple peak activation across memory-selective sites, separately in each condition. We used a time window of -1500 to 1500 relative to the hippocampal ripple peak and standardized the peri-ripple response in each site using a z-score transformation. During the autobio and rest conditions peak latency was not significantly different from zero (peak latencies: autobio, 56 ± 71 ms; 5-sec rest, 64 ± 72 ms). During math however, peri-ripple activation was slightly delayed, peaking 96 ± 28 ms after the hippocampal ripple peak ($P<0.05$, FDR adjusted).

(G) Peri ripple responses in memory-selective cortical sites were comparable across autobio and semantic retrieval (autobio vs semantic: P=NS, cluster-based permutation test; n=118 recording sites from 11 patients who had the semantic condition).

(H-I) In a complementary validation analysis, we computed the ripple-triggered HFB response in memory-selective sites without using a deconvolution model, i.e., by directly time-locking the cortical activity to hippocampal ripples and computing the average. Importantly, we compute this average either using the actual ripple latencies (solid line) or ripple latencies that were shuffled across trials (dashed line). Subtracting the two averages (panel I) uncovered the ripple-coupled component. While completely bypassing the GLM approach, this complementary analysis revealed peri-ripple response that was highly consistent with the deconvolved response described in Figure 6C (Pearson's $r = 0.91$).

Shaded areas represent SEM. Error bars in A and B represent the 95% confidence interval of the within-subject difference.

Table S1. Summary of behavioral performance in each experimental condition, related to STAR Methods

Condition	Reaction time in sec Mean (± SE)	% Correct Mean (± SE)	Number of participants	Number of trials Mean (range)
Autobio.	2.82 (± 0.26)*	N/A	20	73.8 (47-80)
Semantic	2.78 (± 0.17)	86.7 (±2.6)	11	36.8 (36-37)
Math	3.65 (± 0.31)	89 (±1.4)	20	78.9 (71-80)
5s-Rest	N/A	N/A	20	43.6 (29-74)

* This is the grand average reaction time (RT) computed across all participants. However, when including only the sub-group of 11 patients that had both autobio and semantic conditions, the RT in the autobio condition was significantly lower compared to the semantic RT (2.35 ± 0.16 sec; $P<0.001$, Wilcoxon signed rank test).

Table S2. Demographic information, hippocampal electrode coverage and seizure onset zone for each patient, related to STAR Methods

Subject #	Gender	Age	IQ	Handedness	Electrode Laterality	Seizure Onset Zone	Seizure Laterality	Semantic Condition
SUB01	M	26	N/A	R	Bilateral	Posteromedial to medial-frontal	Bilateral	yes
SUB02	F	22	105	R	Bilateral	Insula	R	no
SUB03	M	32	77	R	Bilateral	MTL	L	no
SUB04	F	19	91	R	Bilateral	Lateral temporal	L	yes
SUB05	F	48	71	R	R	MTL	R	yes
SUB06	F	44	82	L	Bilateral	Orbitofrontal	Bilateral	yes
SUB07	M	52	70	R	R	MTL	R	no
SUB08	M	N/A	N/A	R	Bilateral	Multifocal - orbital, insular, temporal	Bilateral	no
SUB09	M	31	61	R	Bilateral	MTL	L	no
SUB10	F	42	92	R	R	MTL	R	yes
SUB11	F	48	109	R	R	Temporal origin	R	yes
SUB12	F	50	85	R	Bilateral	MTL	L	no
SUB13	M	36	N/A	R	Bilateral	Occipital, mesial temporal	L	no
SUB14	F	56	N/A	R & L	Bilateral	Amygdala	L	no
SUB15	F	19	102	R	R	Temporal-occipital	R	yes
SUB16	M	28	78	R	Bilateral	Insula and MTL	Bilateral	yes
SUB17	M	59	96	R	Bilateral	Bilateral MTL	Bilateral	yes
SUB18	F	45	88	R	Bilateral	Premotor	R	yes
SUB19	M	29	112	N/A	Bilateral	Insula	L	yes
SUB20	M	30	87	R	Bilateral	MTL	L	no
		M = 37.7	M = 87.9					

Table S3. Depth electrode dimensions for each patient, related to Figure 1

Subject #	Distance between electrodes	Electrode diameter	Electrode height
SUB01	4-5 mm	0.86 / 1.12 mm	2.29 / 2.41 mm
SUB02	4-6 mm	0.86 mm	2.29 mm
SUB03	3-8 mm	0.86 mm	2.29 mm
SUB04	3-8 mm	0.86 mm	2.29 mm
SUB05	4-6 mm	0.86 mm	2.29 mm
SUB06	5 mm	1.12 / 1.3 mm	1.57 / 2.41 mm
SUB07	5 mm	0.86 mm	2.29 mm
SUB08	5 mm	1.12 mm	2.41 mm
SUB09	3-6 mm	0.86 mm	2.29 mm
SUB10	3-7 mm	0.86 mm	2.29 mm
SUB11	3-5 mm	0.86 mm	2.29 mm
SUB12	5 mm	1.12 mm	2.41 mm
SUB13	3-5 mm	0.86 mm	2.29 mm
SUB14	3-5 mm	0.86 mm	2.29 mm
SUB15	5 mm	0.86 mm	2.29 mm
SUB16	4 mm	0.86 mm	2.29 mm
SUB17	5 mm	1.12 mm	2.41 mm
SUB18	5 mm	1.12 mm	2.41 mm
SUB19	5 mm	1.12 mm	2.41 mm
SUB20	4-7 mm	0.86 mm	2.29 mm

Table S4. Distribution of analyzed recording sites across patients, related to STAR Methods

	Cortical sites (bipolar pairs)				*Hippocampal sites*
Subject #	Total analyzed	Within DMN	Outside DMN	Memory-selective	CA1/CA2-3/subiculum
SUB01	77	35	42	17	4
SUB02	53	13	40	19	7
SUB03	65	21	44	11	7
SUB04	56	14	42	6	10
SUB05	37	7	30	7	9
SUB06	66	26	40	27	3
SUB07	25	4	21	0	3
SUB08	27	9	18	0	2
SUB09	64	18	46	4	4
SUB10	27	7	20	0	3
SUB11	34	12	22	7	5
SUB12	68	19	49	8	6
SUB13	45	7	38	14	3
SUB14	29	13	16	12	6
SUB15	56	13	43	10	4
SUB16	62	22	40	6	10
SUB17	47	11	36	8	12
SUB18	85	24	61	21	5
SUB19	30	9	21	9	2
SUB20	39	12	27	11	7
TOTAL	992	296	696	197	112